Arabian Journal of Chemistry (2023) **16**, 105022

King Saud University

Arabian Journal of Chemistry

www.ksu.edu.sa
www.sciencedirect.com

ORIGINAL ARTICLE

Optimization of lead (II) removal from water and wastewater using a novel magnetic nanocomposite of aminopropyl triethoxysilane coated with carboxymethyl cellulose cross-linked with chitosan nanoparticles

Ahmad Abo Markeb [a,b], Javier Moral-Vico [a], Antoni Sánchez [a], Xavier Font [a,*]

[a] *Department of Chemical, Biological and Environmental Engineering, Escola d'Enginyeria, Universitat Autònoma de Barcelona, 08193 Bellaterra, Spain*
[b] *Chemistry Department, Faculty of Science, Assiut University, 71516 Assiut, Egypt*

Received 13 December 2022; accepted 17 May 2023
Available online 23 May 2023

KEYWORDS

Lead (II) ion;
Wastewater;
Adsorption;
Reuse;
Interaction mechanism;
Response surface methodology

Abstract The removal of heavy metals from industrial wastewater is nowadays one of the most interesting challenges in water remediation using adsorbent nanomaterials. The present study presents a novel adsorbent (Fe_3O_4@CS@CMC-$SiNH_2$) nanocomposite (NC), by functionalization of the carboxymethyl cellulose (CMC) cross-linked to magnetic chitosan nanoparticles (Fe_3O_4@CS NPs) with aminopropyl triethoxysilane layer (APTES), and evaluate its performance toward lead (II) removal from wastewater. The synthesized NCs were characterized using several techniques. The optimization of the adsorption process was performed using the Response Surface Methodology with the Box-Behnken Design model. The optimal conditions for lead (II) ion removal were found to be; pH of 5.1, a dose of 0.10 g/L, and a temperature of 36 ℃ using Fe_3O_4@CS@CMC-$SiNH_2$ NCs which proved to have superior adsorption performance with a maximum adsorption capacity of 555.56 $mg_{Pb(II)}/g_{NC}$, and fast achievement of the adsorption equilibrium (30 min). Favorable monolayer chemisorption was estimated and proved to be a coordination bond between the ═NH amide and lead (II) ions using FTIR, as well as up to seven adsorption–desorption cycles were effective for lead (II) ion removal from aqueous solutions. In addition, the Fe_3O_4@CS@CMC-$SiNH_2$ NCs showed 98.10%, and 97.21 % removal of lead (II) ions in the

* Corresponding author.
E-mail address: xavier.font@uab.cat (X. Font).
Peer review under responsibility of King Saud University.

Production and hosting by Elsevier

https://doi.org/10.1016/j.arabjc.2023.105022

absence, and the presence of other contaminants of heavy metals such as cadmium (II) and mercury (II). Moreover, the Fe_3O_4@CS@CMC-$SiNH_2$ NC exhibited high efficiency in the removal of lead (II) ions from wastewater, can be easily separated from water by magnetic separation, showed satisfactory reusability for five cycles of the adsorption–desorption process of lead (II) ion removal from tap water and wastewater. Consequently, Fe_3O_4@CS@CMC-$SiNH_2$ NC is a prospective adsorbent nanomaterial for lead (II) ions removal from wastewater.

1. Introduction

Due to the increase in human activities and the development of industries all over the world, various compounds from industrial wastewater have been produced and can cause significant harm to some organisms and the environment (Karimi-Shamsabadi and Nezamzadeh-Ejhieh 2016, Huang et al. 2021). Heavy metals are very harmful compounds to be released into the environment in comparison to organic pollutants due to their non-biodegradable behavior and their accumulation in living tissues (Ozdes et al. 2009). These persistent materials can also enter the food chain through water or related ecosystems (Das et al. 2022). Lead is ranked as the second hazardous pollutant after arsenic according to the U.S. Environmental Protection Agency (USEPA) and the Agency for Toxic Substances and Disease Registry (ATSDR) (Maliyekkal et al. 2010). The EPA and the World Health Organization (WHO) define the maximum permissible limit for lead (II) ions in drinking water to be 15 µg/L and 10 µg/L, respectively (Ihsanullah et al. 2016). The lead (II) ion is a highly toxic metal ion and can be found in wastewater from batteries, cosmetics, glass manufacturing and paint industries (Eren et al. 2009, Karatas 2012). The high extent of lead (II) ion exposure causes damage to the nervous system of children, anemia, kidney failure, brain edema and liver cirrhosis (Shi et al. 2009). Furthermore, to eliminate the harmful impact on both terrestrial and aquatic living systems, it is necessary to remove the lead (II) ion from water and wastewater.

Several limitations have been reported for the removal of the lead (II) ion from water via traditional methods such as electrochemistry, precipitation or ion exchange. For instance, low efficiency, high cost, secondary pollutants generation, and poor selectivity are documented by using these common methods (Liu et al. 2020).

Therefore, the adsorption technology has been widely used for heavy metals as well as for the removal of other contaminants from water due to its cost-effectiveness, ease of operation, and eco-friendliness as well as the adsorbent could be regenerated (Renu et al. 2016, Jin et al. 2019). Removal of heavy metals using adsorbent nanomaterials is highly favorable due to the augmentation of active sites as well as the high specific surface area for the adsorption of contaminants (Kolluru et al. 2021). Typical adsorbent materials such as resins, activated carbon, biomaterials and agriculture byproducts, among others, have been applied to remove pollutants from water (Hu et al. 2015, Abo Markeb et al. 2017, Sadegh et al. 2017, Abo Markeb et al. 2019) presenting several disadvantages. For example, magnetite nanoneedles, graphene oxide, magnetic biochar, and activated carbon adsorbents used for lead (II) removal have low adsorption capacity, low selectivity, difficulties for being separated from the aqueous medium, unsatisfactory reusability and low stability (Lee and Yang 2012, Karunanayake et al. 2018, Shi et al. 2019, Singh and Bhateria 2020). Consequently, this study aims to: (1) synthesize two novel nanocomposites (NCs): Fe_3O_4@CS@CMC and Fe_3O_4@CS@CMC-$SiNH_2$, based on the usage of low-cost biopolymers of chitosan and carboxymethyl cellulose materials with high magnetic properties, (2) to determine the properties of the synthesized nanocomposite that show the best efficiency for lead (II) ion removal from water such as morphology, size, stability, and crystallinity via different characterization techniques, (3) to optimize the removal and adsorption capacity of lead (II) ion on Fe_3O_4@CS@CMC and Fe_3O_4@CS@CMC-$SiNH_2$ NCs using the Response Surface Methodology (RSM) with a Box-Behnken Design (BBD), (4) to estimate the parameters related to adsorption of lead (II) on Fe_3O_4@CS@CMC and Fe_3O_4@CS@CMC-$SiNH_2$ NCs via isotherm and kinetic studies, (5) to investigate the adsorption mechanism of lead (II) ion onto the best synthesized NC and (6) to evaluate its potential applications in tap water and wastewater as well as its reusability.

2. Materials and methods

2.1. Materials and characterization

All materials used in this work and details of the nanocomposites' characterization are provided in the supplementary Information (section S1.1).

2.2. Synthesis of Fe_3O_4@CS@CMC and Fe_3O_4@CS@CMC-$SiNH_2$ NCs

Fe_3O_4@CS@CMC and Fe_3O_4@CS@CMC-$SiNH_2$ NCs were prepared using the wet chemical method, which is subsequently explained.

2.2.1. Fe_3O_4@CS@CMC NC synthesis

Briefly, 1 g of chitosan was dissolved in 100 mL distilled water containing 4 mL of acetic acid and left to continuous stirring for 24 h at room temperature. Next, $FeCl_2{\cdot}4H_2O$ (25 mM) and $FeCl_3{\cdot}6H_2O$ (50 mM) were added to the chitosan solution, and the mixture solution was purged using argon gas for 1 h. Then, 0.1 g of CMC was added and the solution was continuously stirred under argon atmosphere for 1 h. After that, the mixture solution was kept stirred for an additional 1 h after the adjustment of the pH of the solution to 9.00 using NaOH (1 M). Finally, the Fe_3O_4@CS@CMC NC was freeze-dried for 48 h after centrifugation and washed three times with Milli-Q water.

2.2.2. Fe_3O_4@CS@CMC-$SiNH_2$ NC synthesis

Fe_3O_4@CS@CMC-$SiNH_2$ NC was prepared as follows: 100 µL of (3-aminopropyl)triethoxysilane (APTES) was added to a suspension of 0.5 g of Fe_3O_4@CS@CMC, previously dispersed into 60 mL of toluene for 30 min, and the mixture was kept under stirring for 4 h at 60 ℃. Finally, the NCs were freeze-dried for 48 h after centrifugation and washed three times with Milli-Q water.

2.3. Adsorption experiments

Lead (II) ion removal using the synthesized nanocomposites was carried out under batch operation mode to determine

the optimal conditions with maximum removal efficiency and adsorption capacity of lead (II) ions from aqueous solutions. A fixed amount of the adsorbent (mg) was mixed with a defined volume and a known concentration of lead (II) ion solution (V_L, mg/L) at a specific pH using an incubating shaker (JSR, Korea) at 180 rpm for a defined time (min). Next, the residual concentration of lead (II) ion solution (C_e) was measured by Atomic Absorption Spectroscopy (AAS) (Contra AA 700, Germany) after digestion of the sample in HNO_3 solution (5%) for 24 h and/or UV/VIS spectrophotometer (PG990 Instruments, UK) after separation of the adsorbent by magnetic separation with a neodymium magnet. Cadmium (II) and mercury (II) were determined using Inductive coupled plasma coupled to optical emission spectroscopy (ICP-OES), and Atomic absorption spectroscopy coupled to thermal decomposition, respectively at Servei d'Anàlisi Química, UAB, Spain. The percent of removal (R, %) and equilibrium uptake capacity of lead (II) ion (Q_e, $mg_{Pb(II)}/g_{NC}$) were calculated using the equations presented in the Supplementary Information (section S1.3).

2.4. Optimization of the lead (II) ion removal using RSM

The optimization study of lead (II) ion removal was designed using the Design Expert Program 12.0.10 (Stat-Ease, USA, 2019), and the RSM with BBD was selected. The three factors used to carry out this study were the pH (A), adsorbent dose (B) and temperature (C). The removal efficiency and the adsorption capacity of lead (II) ions were the response values used as shown in Supplementary Information (Table S1). Three levels were defined for each factor: the low level (coded −1), the center point (coded 0) of the cubic phases ($\alpha = 1$), and the high level (coded + 1), which are included in the BBD. The experiment was conducted with different operating parameters such as pH (2, 6 and 10), dose (0.1, 0.8 and 1.5 g/L), and temperature (20, 35 and 50 ℃). The range of pH from 2 to 10 was selected due to the functional groups on the adsorbent NC, protonated or deprotonated, and the species of the metal ion, which are affected by the pH of the solution. Also, the spontaneous and favorable reaction of the adsorbent with metal ions could be estimated by the effect of temperature. In addition, the evaluation of the adsorption sites on the surface of the NC could be proved by the study by the effect of dose (Zhang et al. 2020). The initial lead (II) ion concentration used was 10 mg/L, which is higher than the maximum permissible concentrations of lead (0.05 mg/L in drinking water according to the World Health Organization, and 0.05 mg/L in wastewater according to the Environmental Protection Agency (Goel et al. 2005)), and the contact time of 24 h was selected to be sure that the equilibrium state between the pollutant and the adsorbent NC was achieved. A total run of 17 experimental points was performed according to the BBD model to find out the optimal conditions for the three variables that result in maximum values of both responses; the adsorption capacity (Y, $mg_{Pb(II)}/g_{NC}$) and the removal efficiency (R, %).

2.5. Adsorption kinetics

To determine the optimum time for the adsorption of lead (II) ion on the NC adsorbents under equilibrium, the experiments of the kinetic study were conducted using 10 mg/L as lead (II) ion initial concentration and doses of 0.11 g/L and 0.10 g/L of Fe_3O_4@CS@CMC and Fe_3O_4@CS@CMC-$SiNH_2$ NCs, respectively, as they were the optimal dosages obtained from the BBD. The interval of time ranged from 5 min to 24 h to assure the achievement of the equilibrium state. Then, the linear form of three kinetics models tested: pseudo-first, pseudo-second and intra-particle diffusion models, was used to estimate the rate of adsorption.

2.6. Adsorption isotherms

To determine the maximum adsorption capacities (Q_{max}, $mg_{Pb(II)}/g_{NC}$) of lead (II) ions using Fe_3O_4@CS@CMC and Fe_3O_4@CS@CMC-$SiNH_2$ NCs, the effect of the initial concentration of lead (II) ions was studied. The adsorption isotherm experiments for both Fe_3O_4@CS@CMC and Fe_3O_4@CS@CMC-$SiNH_2$ NCs were conducted using a range of lead (II) ion concentrations (1 mg/L to 150 mg/L). This range was used to confirm the achievement of the maximum adsorption capacities of lead (II) ion on the surface of the synthesized adsorbents under the optimum conditions of pH, dose and temperature from the BBD study as well as the optimum time for adsorption from the kinetic study. In addition, the experimental data were fitted to three linear models of isotherm: Langmuir, Freundlich and Dubinin-Radushkevich to estimate Q_{max} ($mg_{Pb(II)}/g_{NC}$) and the adsorption mechanism for lead (II) ion removal.

2.7. Regeneration and reusability studies

The regeneration and reusability experiments were performed through two strategies. One is testing the reusability of the adsorbent NC for lead (II) ion removal from an aqueous solution, and the other is testing its reusability in tap water and wastewater. Firstly, the reusability of Fe_3O_4@CS@CMC NC was tested directly after one cycle of lead (II) ions (1 mg/L) adsorption from an aqueous solution under optimum conditions, followed by its usage in two more cycles. Next, Fe_3O_4@CS@CMC and Fe_3O_4@CS@CMC-$SiNH_2$ NCs were subjected to HNO_3 (0.01 M) as a desorbing agent and were incubated under shaking for 2 h at 25 ℃ and 180 rpm after the first cycle of lead (II) ion (1 mg/L) adsorption. Then, the obtained NCs were washed with deionized water three times using magnetic decantation. Thus, the recovered adsorbents were employed for six cycles of lead (II) ion (1 mg/L) adsorption under optimal conditions. Therefore, the ability of the regeneration process was evaluated. Secondly, the reusability of Fe_3O_4@CS@CMC-$SiNH_2$ NC was tested as mentioned after regeneration in three types of water matrices: tap water (Barcelona, Spain) and also the inlet and outlet wastewater supplied from the WWTP of La Garriga (Barcelona, Spain) spiked with lead (II) ion (1 mg/L) for five consecutive cycles of adsorption–desorption tests. Detailed information regarding the analysis of tap water and wastewater matrices is presented in Supplementary Information (section S1.5).

2.8. Statistical data analysis

All the data of the adsorption processes were statistically analyzed, and the polynomial regression models involving the three operational factors: temperature, pH and dosage, were

estimated via ANOVA using the Design Expert Program 12.0.10 (Stat-Ease, USA, 2019). The inclusion of data, righteousness of fit, and its statistical significance were determined using the regression correlation coefficient (R^2), and the p-value. All data in this study were considered statistically significant when the p-values were less than 0.05.

3. Results and discussion

3.1. Structural and microstructural characterization of NCs

3.1.1. HR-TEM analysis

The morphology and size of Fe_3O_4@CS@CMC-$SiNH_2$ NCs were obtained from HR-TEM analysis. As shown in Fig. 1a, the nanocomposite presents a cubic morphology with sizes ranging from 15 nm to 32 nm. The phase identification of the nanocomposites was confirmed using Selected Area Electron Diffraction (SAED) pattern (Fig. 1b), which also shows that crystalline nanocomposites were produced. In addition, Fig. 1a shows the successful introduction of the APTES by the formation of an amino layer coat on the surface of the cubic synthesized nanocomposites. In addition, the particle size of Fe_3O_4@CS@CMC NCs was found to be 13.52 n m ± 2.97 nm using the normal TEM as shown in Fig. S1a.

3.1.2. XRD analysis

The crystallinity and phases of Fe_3O_4@CS@CMC-$SiNH_2$ NCs are shown in Fig. 2. The characteristic peaks in the spectra of Fe_3O_4@CS@CMC-$SiNH_2$ NCs agreed with the formation of magnetite nanoparticles with cubic phases (JCPDS 85–1436) (Cai et al. 2017).

The peaks at 19.18 °, 29.86°, 35.68°, 45.58°, 56.62°, 62.74° and 75.24° were assigned to (111), (220), (311), (400), (511), (440) and (622) reflections (Park et al. 2010, Kurnaz Yetim et al. 2020). In addition, the peaks appeared at 11.56°, 17.08° and 22.66° corresponding to chitosan NPs (Morsy et al. 2019). The peak at 25.18° corresponds to the presence of Si-NH_2 (Xu et al. 2013). Moreover, the sharpness of peaks indicates the crystallinity of the synthesized nanocomposites. In addition, the intensities of some peaks were decreased and disappeared of other peaks such as 62.74°, and 75.24° in the case of Fe_3O_4@CS@CMC NCs as shown in Fig. S1b. Hence, the APTES increases the crystallinity of the synthesized NC.

3.1.3. FTIR analysis

Figure S2 shows the FTIR spectra of Fe_3O_4@CS@CMC and Fe_3O_4@CS@CMC-$SiNH_2$ NCs. The characteristic absorption bands are corresponding to the functional groups of the synthesized nanocomposites. For instance, in the case of Fe_3O_4@CS@CMC-$SiNH_2$ NCs, strong absorption peaks at 3448 cm^{-1} and 1640 cm^{-1} are attributed to the N—H stretching vibration and NH_2 bending mode of the free NH_2 group of chitosan, respectively. The peaks at 3005 cm^{-1} and 2937 cm^{-1} correspond to the asymmetric and symmetric C—H vibration, respectively. The bending vibration absorption peak of —CH_2 appeared at 1439 cm^{-1}. In addition, the absorption peak at 1341 cm^{-1} could be attributed to the —CN stretching. The successful introduction of APTES was confirmed by the presence of the vibration absorption peaks of —NH bending at 1588 cm^{-1} and —CONH at 1640 cm^{-1}, as well as the disappearance of the vibration peak of —OH bending of carboxylic acid at 1425 cm^{-1}. Furthermore, the absorption peak at 546 cm^{-1} presents the characteristics of the stretching vibration of the Fe—O bond. The stretching vibration of —CH_3 in the CMC structure was proved by the appearance of the absorption peak at 2867 cm^{-1}. In addition, the absorption peak at 870 cm^{-1} is assigned to the glycosidic bond in the CMC structure. The absorption peak at 1050 cm^{-1} is attributed to the stretching vibration of the O—C—C bond. The shift of this peak from pure CMC (1043 cm^{-1}) is due to the CMC moieties that have been introduced on the Fe_3O_4 surfaces. Moreover, the peak at 2365 cm^{-1} is assigned to the C═N stretching of chitosan. Therefore, if the absorption peaks of the synthesized materials are compared to the peaks of Fe_3O_4@CMC or CS-SiO_2@Fe_3O_4 nanoparticles (Cai et al. 2017, Danalıoğlu et al. 2018), it can be concluded that novel nanocomposites of Fe_3O_4@CS@CMC-$SiNH_2$ NCs were produced. While in the case of Fe_3O_4@CS@CMC NCs, the intensity of the —CONH was decreased, and the —OH bending of the carboxylic acid of CMC was increased.

3.2. Optimization of the lead (II) removal from aqueous solutions using RSM

The obtained results from the experiment based on the suggested run using the BBD model are listed in Supplementary Information (Table S2). Based on the BBD results, the quadratic model is suitable for the removal efficiency and the adsorption capacity of lead (II) ions using Fe_3O_4@CS@CMC

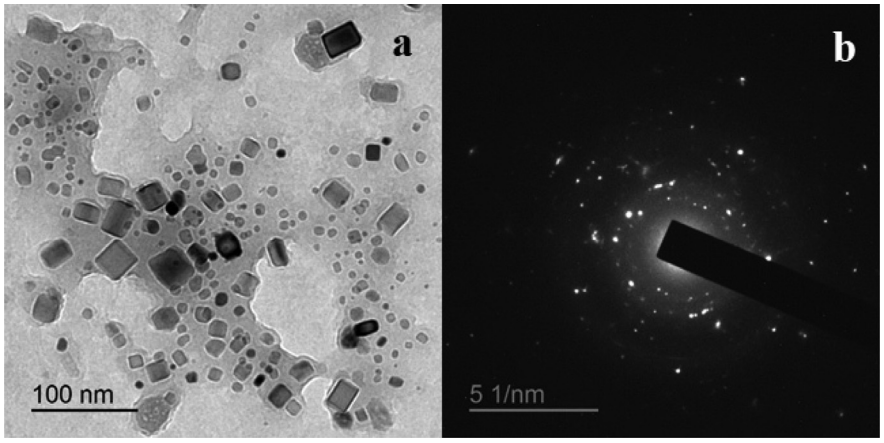

Fig. 1 Figure 1. HR-TEM (a), and SAED (b) images of Fe_3O_4@CS@CMC-$SiNH_2$ NCs.

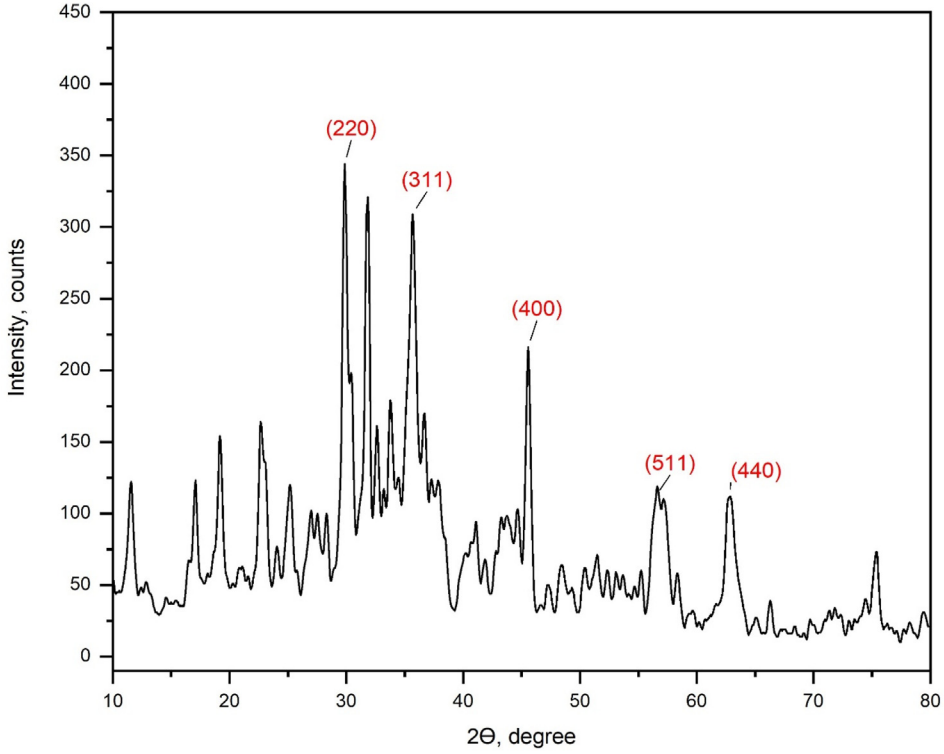

Fig. 2 **Figure 2.** XRD pattern of Fe_3O_4@CS@CMC-$SiNH_2$ NCs.

and Fe_3O_4@CS@CMC-$SiNH_2$ NCs, respectively. Statistical values of R^2 and p-values were found to be 0.9753 and 0.0179 in case of using Fe_3O_4@CS@CMC, and 0.9980 and less than 0.0001 in case of using Fe_3O_4@CS@CMC-$SiNH_2$ NCs, respectively. Also, Tables S3 and S4 demonstrated that the cubic model is adequate for modelling the adsorption capacity, and the removal efficiency of lead (II) ions using Fe_3O_4@CS@CMC and Fe_3O_4@CS@CMC-$SiNH_2$ NCs, respectively. In this case, R^2 and p-values were found to be 0.9999 and less than 0.0001 in case of using Fe_3O_4@CS@CMC, and 0.9931 and 0.001 in case of using Fe_3O_4@CS@CMC-$SiNH_2$ NCs. The significance of each coefficient to demonstrate the interactions between the variables was examined using the p-values. As shown in Tables S3 and S4, for the response of removal efficiency of lead (II) ions from aqueous solutions, the factors A, B, and B^2 are significant in the case of using Fe_3O_4@CS@CMC NC, whereas the factors A, AB, A^2, B^2, C^2, A^2B, and AB^2 are significant in case of Fe_3O_4@CS@CMC-$SiNH_2$ NCs. Moreover, the factors of A, B, C, AB, AC, BC, A^2, B^2, C^2, A^2B, A^2C, and AB^2 are significant using Fe_3O_4@CS@CMC NC and B and B^2 are the significant factors using Fe_3O_4@CS@CMC-$SiNH_2$ NCs for the response of the adsorption capacity of lead (II) ions. Therefore, the final obtained equations in terms of the coded factors are shown in Eqs. (3)–(6):

$$R1(\%) = 98.47 + 17.69A + 27.02B - -23.25B^2 \quad (3)$$

$$Q1\left(mg_{Pb(II)}/g_{NC}\right) = 12.31 + 0.98A - -6.32B + 6.1C - - 21.55AB + 1.26AC - 6.35BC + 7.26 A^2 + 10.5B^2 - -10.14C^2 - -18.00A^2 + 10.50B^2 - - 10.14C^2 - -18.00A^2B - -6.96A^2C + 21.33AB^2 \quad (4)$$

$$R2(\%) = 95.54 + 13.79A + 7.32AB - -6.71A^2 + 4.25B^2 - -7.46C^2 - 4.20A^2B - -11.32AB^2 \quad (5)$$

$$Q2\left(mg_{Pb(II)}/g_{NC}\right) = 11.82 - -43.26B + 38.39B^2 \quad (6)$$

where R1, and R2 are the removal efficiencies (%), and Q1 and Q2 are the lead (II) adsorption capacities ($mg_{Pb(II)}/g_{NC}$) using Fe_3O_4@CS@CMC and Fe_3O_4@CS@CMC-$SiNH_2$ NCs, respectively. A, B, and C are the factors used in the optimization, i.e., pH, dose (g/L), and temperature (℃), respectively. The positive coefficient terms mean a positive contribution to the removal process of lead (II) ions from aqueous solutions using Fe_3O_4@CS@CMC and Fe_3O_4@CS@CMC-$SiNH_2$ adsorbents. In addition, the higher coefficients, among the terms that are positively charged, suggest that the pH and the adsorbent dose have a great impact on lead (II) adsorption (Afolabi et al. 2021). The ANOVA results of the quadratic and cubic models for lead (II) ion removal from aqueous solution as well as its adsorption capacity using Fe_3O_4@CS@CMC and Fe_3O_4@CS@CMC-$SiNH_2$ NCs are shown in the Supplementary Information (Tables S3 and S4, respectively). The F-values for the two models were found to be 5.46, and 73.45E + 03, using Fe_3O_4@CS@CMC for the removal and adsorption capacity, respectively (Table S3). Also, Table S4 shows 48.11, and 385.04 as the F-values for the two models for the removal and adsorption capacity, respectively using Fe_3O_4@CS@CMC-$SiNH_2$ NCs. These values indicate the significance of the obtained models, in which p-values are lower than 0.05. In the quadratic equations, the lack of fit was 1190.58 for the lead (II) removal using Fe_3O_4@CS@CMC NC and 317.53 for the lead (II) adsorption capacity using Fe_3O_4@CS@CMC-$SiNH_2$ NC as presented in Tables

S3 and S4, respectively. Accordingly, each model was suitable enough to describe the results of the experimental analysis (p-values lower than 0.05). Therefore, the removal percentage of lead (II) ions, as well as the adsorption capacity, can be calculated from the equations obtained and can be applied for estimating the capacity of removing lead (II) ions from real aqueous media. Fig. 3 and Fig. S1 displayed the response surface graphs for both responses of removal efficiency and adsorption capacity versus dose, pH and temperature factors, respectively. These responses were obtained by varying two factors, while the third factor is maintained constant at the central level (Dermanaki Farahani and Zolgharnein 2021). As can be seen, the interaction between factors was clearly shown in these plots.

Fig. 3a-c and Fig. 3d-f depict the effects of the parameters that affect the removal of lead (II) ions from water using Fe_3O_4@CS@CMC and Fe_3O_4@CS@CMC-$SiNH_2$ NCs, respectively. Fig. 3a and Fig. 3d show the effect of pH and dose on the removal percentage of lead (II) ions. As shown in Fig. 3a, the lead (II) ion removal increased by increasing the adsorbent dosage from 0.1 to 1.5 g/L using Fe_3O_4@CS@CMC, which can be attributed to the increase of the active sites of the adsorbent. On the contrary, the dose did not show the significance for lead (II) ion removal from aqueous solutions using Fe_3O_4@CS@CMC-$SiNH_2$ NCs in the range of 0.1 to 1.5 g/L, which could be attributed to the presence of high available adsorption active sites in the low dose that could adsorb easily an aqueous solution of lead (II) ion (10 mg/L), and hence the Fe_3O_4@CS@CMC-$SiNH_2$ NCs could adsorb higher amounts of lead (II) ions. In both cases, the removal of lead (II) ions increases when pH increases. This can be attributed to the fact that at low pH, there is an excess of protons that could interfere with the lead (II) ion for the exchange on the surface of the adsorbents (Singh and Bhateria 2020). Moreover, pH increase enhances the removal of lead (II) ions due to the increase of the negatively charged medium as a result of the presence of hydroxyl ions (Davodi et al. 2020).

Fig. 3b and 4e show the effect of temperature and dose on lead (II) removal. A positive effect can be observed by increasing the dose using Fe_3O_4@CS@CMC NC and increasing the efficiency of removal by increasing the temperature up to 36 ℃ using Fe_3O_4@CS@CMC-$SiNH_2$ NC. In addition, Fig. 3c and 3f demonstrate higher efficiency when increasing pH in both NCs. This could be attributed to the high interaction between the lead (II) ion and the synthesized nanocomposites because of the more negatively charged medium.

In summary, the optimal conditions of the selected factors from the analysis are the following: pH of 10 and 5.1, a dose of 0.11 g/L and 0.10 g/L, and temperature of 41.5 ℃ and 36 ℃ for Fe_3O_4@CS@CMC and Fe_3O_4@CS@CMC-$SiNH_2$ NCs, respectively. These conditions were selected for the rest of further adsorption experiments with real water and wastewater. The obtained results are in agreement with those presented in the literature (Ozdes et al. 2009, Rodríguez et al. 2018), where the adsorption of lead (II) ions could be via an ion exchange mechanism in which the lead (II) ions can bind to the anionic sites by replacing the existing metal such as sodium at high pH values as occurred using Fe_3O_4@CS@CMC or via a complexation mechanism as a result of the amino layer that could coordinate with lead (II) ion in case of using Fe_3O_4@CS@CMC-$SiNH_2$ NCs.

3.3. Effect of time and adsorption kinetics as well as the amount of CMC

The adsorption controlling step and the adsorption mechanism can be estimated from the adsorption kinetic modeling. Fig. 4 shows the effect of time on the removal efficiency of lead (II) ions using Fe_3O_4@CS@CMC and Fe_3O_4@CS@CMC-$SiNH_2$ NCs. It was observed that Fe_3O_4@CS@CMC-$SiNH_2$ NCs achieved fast adsorption and equilibrium state in

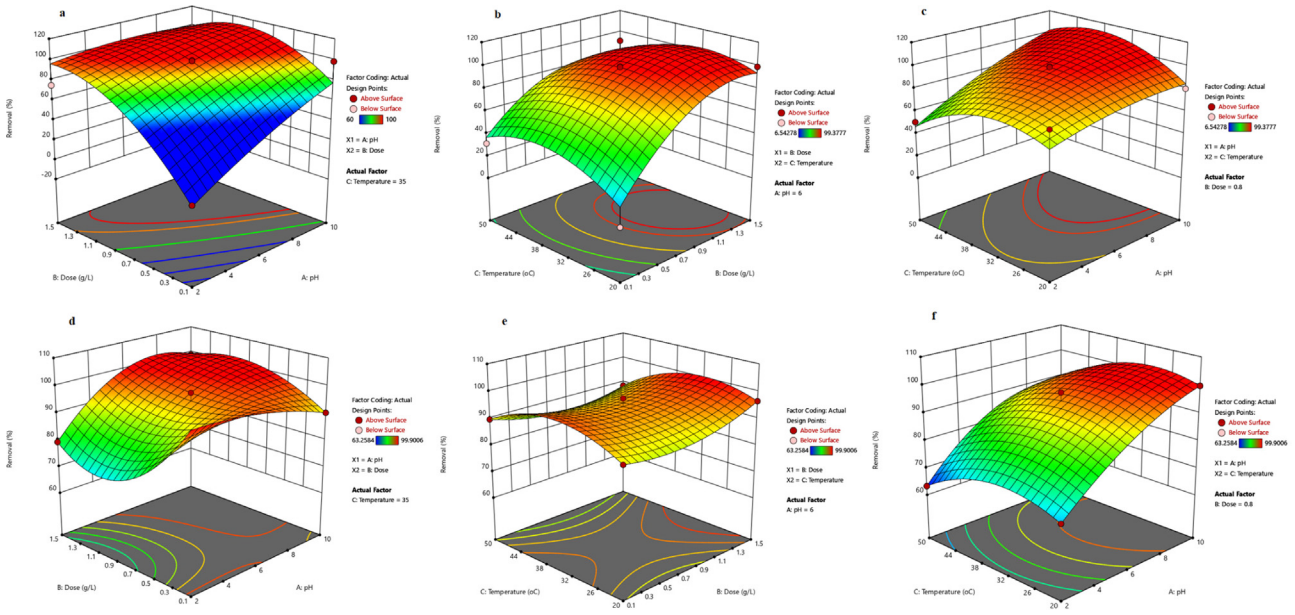

Fig. 3 **Figure 3.** Response surface plots of lead (II) ion removal efficiencies using three variables; (a-c) using Fe_3O_4@CS@CMC, and (d-f) Fe_3O_4@CS@CMC-$SiNH_2$ NCs. Reaction conditions: Initial concentration of lead (II) ion = 10 mg/L and contact time = 24 h.

30 min, whereas a longer time (120 min) was needed in the case of Fe_3O_4@CS@CMC NCs. The equilibrium is stable once reached (Fig. 4).

According to Table S5, three adsorption kinetic models were used: pseudo-first order, pseudo-second order and intra-particle diffusion models. The rate constants of the models, K_1, K_2, and K_{id} were calculated from the slope and intercept of their relevant linear plots as illustrated in Supplementary Information (Figure S3).

The experimental data were tested for the best fitting between the pseudo-first order and pseudo-second order models. As shown in Table S5, The R^2 values were found to be 0.9995 and 0.9954 for the pseudo-second order and pseudo-first order models, respectively, using Fe_3O_4@CS@CMC-$SiNH_2$ NCs. Also, using Fe_3O_4@CS@CMC NCs, the R^2 value of the pseudo-second order model (R^2 = 0.9999) was found to be higher than the pseudo-first order model (R^2 = 0.7183). In consequence, the pseudo-second order model was the most adequate model to describe the experimental data. Therefore, chemisorption is probably the rate-controlling step of adsorption according to the literature (Gong et al. 2012, Yang et al. 2019, Huang et al. 2022). In addition, the experimental adsorption capacity values, Q_e ($mg_{Pb(II)}/g_{NC}$), using Fe_3O_4@CS@CMC and Fe_3O_4@CS@CMC-$SiNH_2$ NCs are in agreement with the calculated Q_e values from the pseudo-second order model (Table S5).

Moreover, the adsorption capacities of lead (II) ion (Q_e) were evaluated under the optimum conditions of pH, dose, temperature, and contact time using Fe_3O_4@CS@CMC-$SiNH_2$ NCs and different amounts of CMC during the synthesis protocol. It was found that the values of Q_e were approximately constant with increasing the amount of CMC from 0.05 g to 0.2 g. For instance, 96.45 mg/g, 97.34 mg/g, and 97.26 $mg_{Pb(II)}/g_{NC}$ were obtained when 0.05 g, 0.1 g, and 0.2 g of CMC, respectively. Therefore, 0.1 g of CMC was selected for the rest of the studies in this work, and future studies could be performed to study the effect of the weight ratio between chitosan and CMC on the removal of lead (II) ions.

3.4. Adsorption isotherms

Three adsorption isotherms models: Langmuir, Freundlich and Dubinin-Radushkevich (DR), were tested to find the maximum adsorption capacity of lead (II) ion. Significant information on the surface properties, affinities of the adsorbents, as well as adsorption mechanism, can be obtained from the isotherm models. Fig. 5 shows the adsorption isotherms of lead (II) ions using Fe_3O_4@CS@CMC and Fe_3O_4@CS@CMC-$SiNH_2$ NCs from the equilibrium experimental data. Moreover, the linear equations, plots, parameters and correlation regression coefficients are presented in the Supplementary Information (Table S6 and Figure S4), where, K_L, K_F and β are the isotherm constants, and q_s and q_{max} are the maximum adsorption capacities ($mg_{Pb(II)}/g_{NC}$) from Dubinin-Radushkevich and Langmuir models, respectively. The Langmuir isotherm model fits the experimental data of lead (II) ion adsorption from aqueous solutions with high correlation coefficients: R^2 = 0.9942 (Fe_3O_4@CS@CMC NC) and R^2 = 0.9981 (Fe_3O_4@CS@CMC-$SiNH_2$ NC). The low values of the Langmuir constant (K_L) reflect the strong affinity of the Fe_3O_4@CS@CMC (K_L = 0.325) and Fe_3O_4@CS@CMC-$SiNH_2$ (K_L = 0.353) NCs to lead (II) ions. In addition, one of the important features of the isotherm model is the equilibrium parameter or separation factor (R_L), which is a dimensionless constant. If the values of R_L are 0 or 1, the adsorption is irreversible or linear. The adsorption is favorable

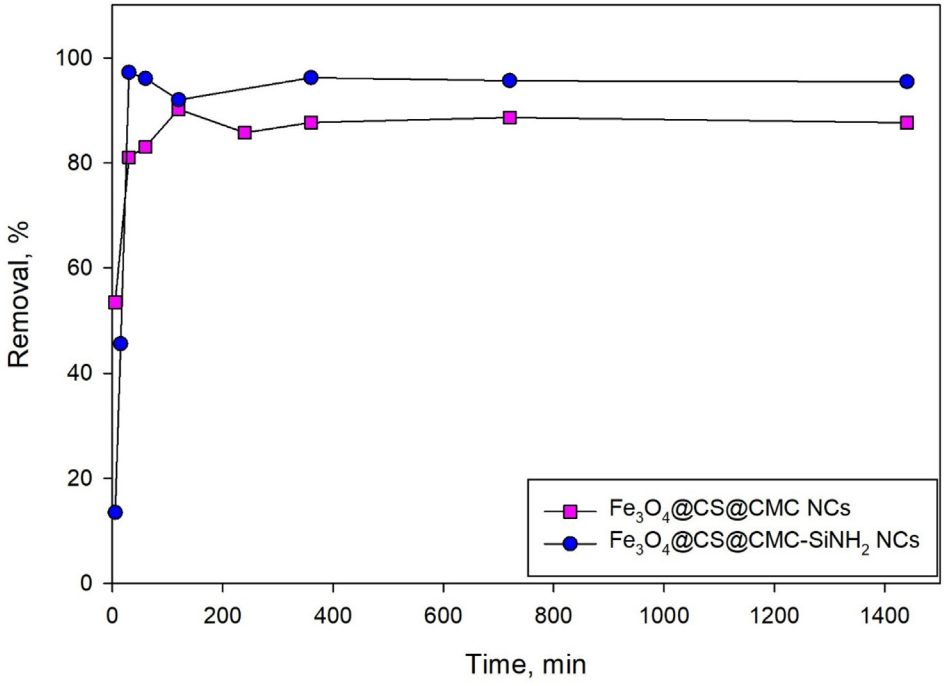

Fig. 4 **Figure 4.**Adsorption kinetics of lead (II) ion removal (10 mg/L) using Fe_3O_4@CS@CMC and Fe_3O_4@CS@CMC-$SiNH_2$ NCs.

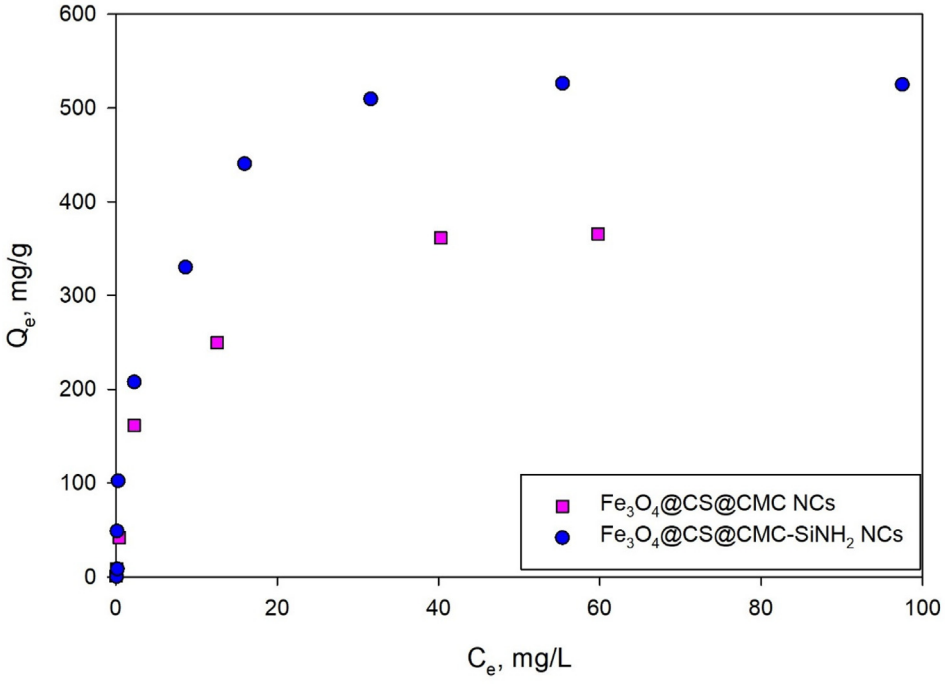

Fig. 5 **Figure 5.**Adsorption isotherms of lead (II) ion removal using Fe_3O_4@CS@CMC and Fe_3O_4@CS@CMC-$SiNH_2$ NCs.

for $0 < R_L < 1$ and unfavorable for $R_L > 1$. For the Fe_3O_4@CS@CMC NCs, the values of R_L range between 0.03 and 0.97, and for Fe_3O_4@CS@CMC-$SiNH_2$ NCs, the values of R_L range between 0.02 and 0.96, which are below 1. Therefore, favorable adsorption exists due to the high affinity between the synthesized NCs and the lead (II) ions, and the monolayer chemisorption between lead (II) ions and the Fe_3O_4@CS@CMC and Fe_3O_4@CS@CMC-$SiNH_2$ NCs (Singh and Bhateria 2020). Furthermore, the maximum adsorption capacities were found to be 384.62 $mg_{Pb(II)}/g_{NC}$ and 555.56 $mg_{Pb(II)}/g_{NC}$ using Fe_3O_4@CS@CMC and Fe_3O_4@CS@CMC-$SiNH_2$ NCs, respectively.

The data analysis using the Freundlich isotherm model, which is mainly validated for multilayer adsorption and heterogenous surface adsorption, is also presented in Table S6. The values of the Freundlich constant (K_F), which denotes the lead (II) ion adsorption capacity, were 52.37 and 138.12 for Fe_3O_4@CS@CMC and Fe_3O_4@CS@CMC-$SiNH_2$ NCs, respectively. The adsorption intensity of the process was evaluated by the values of 1/n and n. As shown in Table S6, the Fe_3O_4@CS@CMC demonstrated values of 0.58 and 1.73 for 1/n and n, respectively. For Fe_3O_4@CS@CMC-$SiNH_2$ NCs, the values of 1/n and n were found to be 0.35 and 2.84, respectively. Therefore, Fe_3O_4@CS@CMC-$SiNH_2$ NCs proved higher interaction with lead (II) ions due to the lower value of 1/n and the maximum value of n in comparison to Fe_3O_4@CS@CMC NCs values.

Besides, the type of adsorption mechanism could be recognized using Dubinin-Radushkevich (DR) isotherm model. For instance, if the adsorption free energy (E) is less than 8 kJ/mol, then physisorption is the predominant mechanism. The calculation of E is presented in Table S6, where it can be deduced that the proposed mechanism is chemisorption due to the free energy values of 11.18 kJ/mol and 12.91 kJ/mol for Fe_3O_4@CS@CMC and Fe_3O_4@CS@CMC-$SiNH_2$ NCs, respectively.

3.5. Regeneration and reusability studies

The reusability tests were performed first using Fe_3O_4@CS@CMC NC for three consecutive cycles of lead (II) ion adsorption (1 mg/L) from aqueous solutions without regeneration of the adsorbent under the optimum conditions of pH, dose, temperature and time as discussed before. In this case, a sharp decrease can be observed in the removal efficiency of lead (II) ions from aqueous solution, which values were 93.03 %, 72.93 % and 60.23 % removed after the first, the second and the third cycles, respectively, as shown in Supplementary Information (Figure S5). This could be attributed to the decrease of the active sites of the adsorbent, decreasing the interaction between the functional groups of the NC and lead (II) ion. However, enhancement of the reusability was proved after regeneration of Fe_3O_4@CS@CMC NC with nitric acid (0.01 M) that desorbs the lead (II) ions from the surface of the adsorbent nanomaterials and hence regenerates the active sites of the NC as presented in Fig. 6. The reason is that nitric acid was highly efficient for lead (II) desorption as reported in the literature (Gong et al. 2005, Patel 2021). Fe_3O_4@CS@CMC NC shows a slight decrease in the removal efficiency up to five cycles (93.03% to 88.29%), and then it shows a decrease with saturation in the efficiencies of removal in the case of cycles six and seven with values of 73.31%, and 74.11%. Moreover, the adsorption performance of Fe_3O_4@CS@CMC-$SiNH_2$ NC demonstrates stable efficiency for seven cycles of adsorption–desorption with a slight decrease in the removal efficiencies (Fig. 6) which is very important from the economical point of view for water treatment in comparison

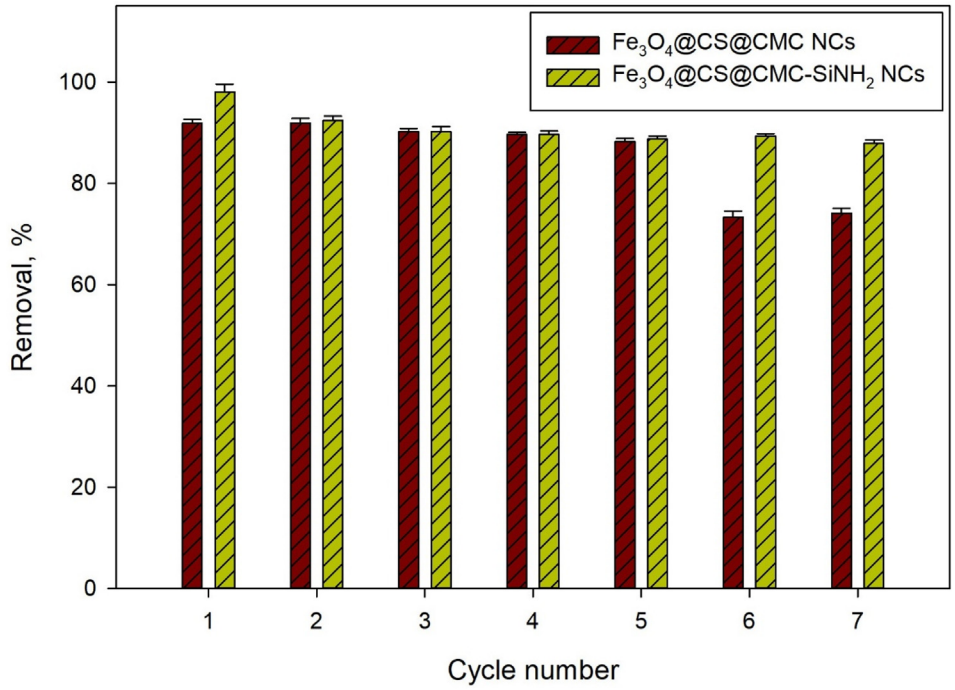

Fig. 6 **Figure 6.**Efficiency of Fe_3O_4@CS@CMC and Fe_3O_4@CS@CMC-$SiNH_2$ NCs after seven adsorption-desorption cycles of lead (II) ion (1 mg/L) removal from aqueous solution.

Table 1 Efficiencies of Fe_3O_4@CS@CMC and Fe_3O_4@CS@CMC-$SiNH_2$ NCs toward tap water, and wastewater applications.

Analyte	Characteristics of water			Removal (%) using Fe_3O_4@CS@CMC NC			Removal (%) using Fe_3O_4@CS@CMC-$SiNH_2$ NC		
	Wastewater Inlet	Wastewater Outlet	Tap water	Wastewater Inlet	Wastewater Outlet	Tap water	Wastewater Inlet	Wastewater Outlet	Tap water
pH	7.40 ± 0.06	7.22 ± 0.03	8.05 ± 0.05	10.0 ± 0.02	10.0 ± 0.02	10.0 ± 0.02	5.10 ± 0.01	5.10 ± 0.01	5.10 ± 0.01
Lead (II)	N.D	N.D	N.D	86.3 ± 0.3	87.8 ± 0.2	88.2 ± 0.4	88.4 ± 0.6	89.9 ± 0.1	91.1 ± 0.4
Chloride	242.7 ± 1.4	227.9 ± 0.6	94.8 ± 0.4	2.7 ± 0.2	7.1 ± 0.3	15.0 ± 0.4	8.3 ± 0.2	15.6 ± 0.3	35.8 ± 0.1
Sulfate	109.8 ± 0.5	78.6 ± 0.2	72.9 ± 0.1	14.4 ± 0.3	3.2 ± 0.1	0.4 ± 0.1	2.5 ± 0.1	12.2 ± 0.2	9.2 ± 0.2
Nitrite	5.5 ± 0.1	3.8 ± 0.1	6.4 ± 0.2	10.0 ± 1.1	26.0 ± 0.6	30.3 ± 0.3	4.1 ± 0.2	9.7 ± 0.1	8.5 ± 0.3
Nitrate	14.1 ± 0.3	10.9 ± 0.2	8.7 ± 0.1	0.11 ± 0.03	1.4 ± 0.2	1.0 ± 0.1	0.0	0.0	0.0
Phosphate	14.9 ± 0.2	5.0 ± 0.2	N.D	22.4 ± 0.4	45.0 ± 0.5	N.D	84.3 ± 0.8	100.0 ± 1.1	N.D
Total organic carbon	69.7 ± 0.5	2.8 ± 0.1	51.0 ± 0.6	13.9 ± 0.1	9.1 ± 0.2	38.4 ± 0.4	98.5 ± 0.6	72.9 ± 0.4	96.5 ± 0.6
Total nitrogen	58.6 ± 0.4	6.27 ± 0.2	2.4 ± 0.2	25.9 ± 1.2	3.0 ± 0.1	2.0 ± 0.2	21.9 ± 1.1	3.7 ± 0.3	2.1 ± 0.2

to the reported studies (Rajput et al. 2016, Bao et al. 2017, Perez et al. 2019, Singh and Bhateria 2020). Thus, Fe_3O_4@CS@CMC-$SiNH_2$ NC was selected for recyclability tests in tap water and wastewater matrices applications.

3.6. Removal of lead (II) from tap water and wastewater

The efficiency of the synthesized adsorbents toward lead (II) removal from tap water, and the wastewater was demonstrated by spiking 1.0 mg/L as a result of the non-detectable lead (II) ion in the real water matrices. Thus, Table 1 exhibits the main characteristics of water (before the spiking of lead (II) ion and applying the optimum conditions for the adsorption process as well as the percentage removal of lead (II) ions as well as other parameters of tap water and wastewater such as nutrients, total organic carbon, salts of chloride and sulfate, and total nitrogen. It can be observed that Fe_3O_4@CS@CMC-$SiNH_2$ NCs have higher efficiency in the lead (II) ion removal from the water matrices than Fe_3O_4@CS@CMC NCs. The decrease in the removal efficiency of lead (II) ions in tap water and wastewater in comparison to its removal from aqueous solution could be attributed to the matrix effect. Also, the efficacy of the Fe_3O_4@CS@CMC-$SiNH_2$ NC was extended to demonstrate the removal of other components from wastewater such

Table 2 Comparison of maximum adsorption capacity, Q_m, between Fe_3O_4@CS@CMC and Fe_3O_4@CS@CMC-$SiNH_2$ NCs and adsorbents studied in the literature.

Nanomaterials	Q_m ($mg_{Pb(II)}/g_{NC}$)	References
Fe_3O_4@CS@CMC@Si-NH_2	555.56	This work
Fe_3O_4-Glu-PDA	389.54	(Mahmoud et al. 2016)
UiO-66-ATA(Zr)	386.98	(Xiong et al. 2020)
Fe_3O_4@CS@CMC	384.62	This work
[2-AA]$CoCl_3$ MIL	344.80	(Abdi Hassan et al. 2022)
GO/SiO_2/Fe_3O_4	333.30	(Burakov et al. 2018)
Mercaptoamine-functionalized silica-coated magnetic NPs (MAF-SCMNPs)	292.00	(Bao et al. 2017)
MnO_2-F-Chitosan	279.72	(Mahmoud et al. 2021)
B-CD@MRHC	266.20	(Liu et al. 2022)
TA@MNPs	210.50	(Das et al. 2022)
Activated Carbon and baker's yeast	151.31	(Mahmoud et al. 2012)
Fe_3O_4-SO_3H	108.93	(Chen et al. 2017)
Water-soluble Fe_3O_4 NPs	96.80	(Wang et al. 2012)
Ultrafine mesoporous Fe_3O_4 NPs	85.00	(Fato et al. 2019)
Fe_3O_4 NPs	81.60	(Recillas et al. 2011)
Fe_3O_4@SiO_2@PPy	65.09	(Mehdinia et al. 2020)
TiO_2/SiO_2/Fe_3O_4-PAA	42.34	(Chu et al. 2019)
Activated carbon	24.32	(Mahmoud et al. 2012)
L-Cyst- Fe_3O_4 NPs	23.88	(Bagbi et al. 2017)
Cellulose- based bio-adsorbents	5.40	(Jaihan et al. 2022)
CdZnS/ZnS quantum dots	3.56	(Yasmeen et al. 2022)

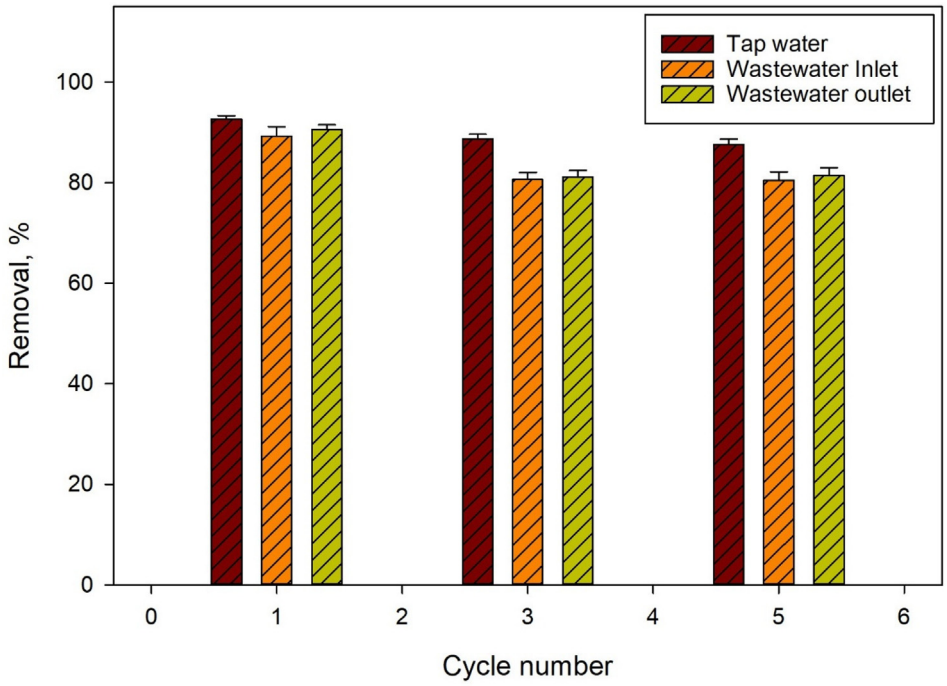

Fig. 7 **Figure 7.**Efficacy of Fe_3O_4@CS@CMC-$SiNH_2$ NCs after five adsorption-desorption cycles of lead (II) ion (1 mg/L) removal from spiked tap water, inlet and outlet wastewater.

as chloride, phosphate and total organic carbon analysis in comparison to Fe_3O_4@CS@CMC NCs as displayed in Table 1.

In addition, a comparison study of the maximum adsorption capacity between the synthesized nanocomposites and the adsorbent nanomaterials reported in the literature is presented in Table 2.

It can be observed that Fe_3O_4@CS@CMC and Fe_3O_4@CS@CMC-$SiNH_2$ NCs present adsorption capacities of lead (II) ions of 384.62 $mg_{Pb(II)}/g_{NC}$ and 555.56 $mg_{Pb(II)}/g_{NC}$, respectively, which are considerably higher than most of the reported in the literature. The high values of Q_m could be attributed to the multifunctional properties of the synthesized adsorbents with ammine and carboxyl functional groups that

could enhance the formation of coordination bonds between the lead (II) ions and the donor atoms as well as a higher number of active sites for lead (II) ions (Shoukry and Hosny 2012, Bao et al. 2017). Moreover, the synthesized adsorbent nanomaterials offer magnetic separation due to the presence of magnetite nanoparticles, which can reduce the cost of water treatment instead of using an alternative methodology to separate the treated water and the adsorbent nanocomposites (Abo Markeb et al. 2019).

3.7. Recyclability studies of Fe_3O_4@CS@CMC-$SiNH_2$ NCs toward tap water and wastewater

Spiked tap water, inlet, and outlet wastewaters were spiked with 1 mg/L of lead (II) ions and subjected to five adsorption–desorption cycles. As shown in Fig. 7, 92.66 % to 87.64 %, 89.25 % to 80.53 % and 90.56 % to 81.46 % adsorption values were obtained when Fe_3O_4@CS@CMC-$SiNH_2$ NCs were applied to five adsorption–desorption cycles for tap water, inlet and outlet wastewater, respectively. The slight decrease in the removal efficiency could be attributed to some of the active sites on the Fe_3O_4@CS@CMC-$SiNH_2$ NCs being occupied by lead (II) ion or other analytes from the water matrices that could not be completely desorbed. Hence, based on the recyclability studies after the regeneration, Fe_3O_4@CS@CMC-$SiNH_2$ NC can be used as an economic and efficient adsorbent for the removal of lead (II) ions from wastewater as well as from tap water. In addition, the desorbed lead (II) ion can be used in industrial applications such as the manufacturing of batteries, which can be conducted in future studies (Bao et al. 2017). Also, the recyclability tests could be further studied in the future with higher concentrations of lead (II) ions spiked into water matrices.

3.8. Selectivity tests

The removal of heavy metals using adsorbent nanomaterials with higher selectivity is great implications for the water treatment process. The selectivity tests were carried out in single and mixed solutions containing 10 mg/L of each heavy metal;

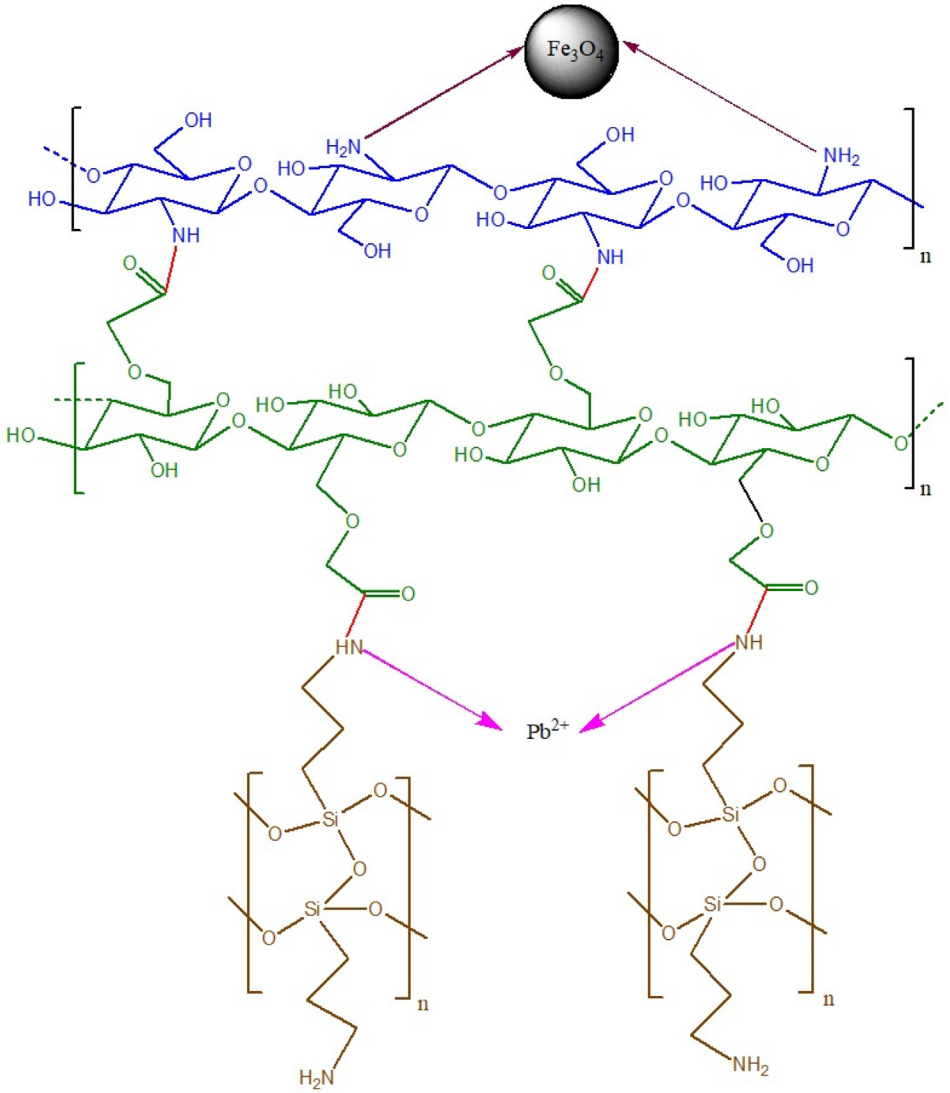

Fig. 8 **Figure 8.**Schematic illustration of the proposed adsorption mechanism of lead (II) ion on Fe_3O_4@CS@CMC-$SiNH_2$ NCs.

Cd(II), Hg(II), and Pb(II) ions to investigate the effect of other inorganic contaminants on the lead (II) ions removal. The results proved that the Fe_3O_4@CS@CMC-$SiNH_2$ NCs could remove individually 98.10 % of Pb(II), and 15.79 % of Hg (II) ions, and it did not show any removal for Cd(II) ions. Moreover, higher selectivity for lead (II) removal from the aqueous solution was observed in the presence of other contaminants such as cadmium (II) and mercury (II) ions. For instance, 97.21%, and 14.74 % of the removal were obtained for Pb(II), and Hg(II) ions, respectively. Therefore, the Fe_3O_4@CS@CMC-$SiNH_2$ NCs proved their efficacy towards the elimination of lead (II) with high selectivity due to the closeness of the removal percentage of lead (II) ions in single and multi-heavy metals solution.

3.9. Adsorption mechanism

As previously explained, Fe_3O_4@CS@CMC-$SiNH_2$ NCs were shown to have better efficiency toward lead (II) ion adsorption in terms of maximum adsorption capacity, applications to tap water and wastewater as well as its regeneration and reusability. Therefore, it is important to elucidate the possible interaction mechanism between the lead (II) ion and Fe_3O_4@CS@CMC-$SiNH_2$ NCs. Figure S6 shows the zeta potential value of Fe_3O_4@CS@CMC-$SiNH_2$ NCs. The zeta potential is a significant method for understanding the surface of nanoparticles and their stability in solution. If zeta potentials are higher than ± 30 mV, they will have high stability (Singh and Bhateria 2020). The synthesized nanocomposites show good stability with values of −42.8 mV, which indicates the negative surface charge of Fe_3O_4@CS@CMC-$SiNH_2$ NCs. In addition, a further demonstration of this chemical interaction was illustrated in Fig. S2c. As shown, the intensity of the ═NH absorption peak was decreased with a slight shift to a higher wavenumber after the interaction with lead (II) ions. Hence, as illustrated in Fig. 8, a chemical interaction between the lead (II) ions and the synthesized nanocomposites is established by the formation of the complex (Li et al. 2019, Huang et al. 2022). The obtained results of coordination between the amide group and the heavy metals are in agreement with the reported one (Dong et al. 2022).

Moreover, SEM pictures of the Fe_3O_4@CS@CMC-$SiNH_2$ NCs before and after the adsorption of lead (II) ions are presented in the Supplementary Information (Figures S7 and S8). The increase in the white part of Figure S7 is a result of the lead (II) ion adsorption on the surface of the nanocomposites. The appearance of the peak at 2.3 keV in the Supplementary Information (Figure S8) corresponds to the lead (II) ion. Therefore, the adsorption process via a complex formation between the –NH amide functional group of the nanocomposite and the lead (II) ion seems the main mechanism of adsorption as presented in Fig. 8. Also, the structural stability of the Fe_3O_4@CS@CMC-$SiNH_2$ NCs after regeneration was studied using XRD to evaluate its property of crystallinity (Figure S9). It was illustrated that the NCs were still crystalline, and the intensities of the peaks decreased. This could be attributed to the effect of nitric acid as a desorbing agent. Therefore, the NC could be potentially applied for further lead (II) ion adsorption process.

4. Conclusions

A novel adsorbent nanomaterial, Fe_3O_4@CS@CMC-$SiNH_2$ NC, has been synthesized in this work, demonstrating a high efficiency for lead (II) ion removal from tap water and wastewater. Cubic morphology with sizes ranging from 15 nm to 32 nm, crystalline and several functional groups as well as stable NC have been demonstrated using characterization techniques. Adsorption processes and RSM with BBD have been applied for the optimization of lead (II) ions removal from water using the synthesized adsorbent nanomaterials. The pseudo-second-order with fast equilibrium within half an hour was found to be the best-fitting model with the experimental data. Besides, favorable monolayer chemisorption was obtained with a maximum adsorption capacity of 555.56 $mg_{Pb(II)}/g_{NC}$ using Fe_3O_4@CS@CMC-$SiNH_2$ NC. Future studies could be performed for further information about the different efficiencies of the two synthesized NCs by evaluating the surface area using BET analysis. Also, future FTIR analysis could be performed to understand the mechanism of interaction between the lead (II) ions and the NCs without modifications by using APTES. Moreover, high efficiency of the adsorbent, Fe_3O_4@CS@CMC-$SiNH_2$ NC, was proved for seven adsorption–desorption cycles of lead (II) ion (1 mg/L) removal from aqueous solution as well as five adsorption–desorption cycles of spiked lead (II) ion (1 mg/L) into drinking water and wastewater. Therefore, the high uptake adsorption capacity and the magnetic separation of Fe_3O_4@CS@CMC and Fe_3O_4@CS@CMC-$SiNH_2$ NCs towards lead (II) ions indicate that the adsorbents under investigation could be used as potential adsorption nanomaterials for lead (II) ion removal from polluted drinking water and wastewater.

CRediT authorship contribution statement

Ahmad Abo Markeb: Conceptualization, Methodology, Investigation, Writing – original draft, Validation. **Javier Moral-Vico:** Writing – review & editing. **Antoni Sánchez:** Writing – review & editing. **Xavier Font:** Supervision, Writing – review & editing.

Declaration of Competing Interest

The authors declare the following financial interests/personal relationships which may be considered as potential competing interests: [Antoni Sanchez reports financial support was provided by Ramon Areces Foundation. Ahmad Abo Markeb reports financial support was provided by Ministry of Higher Education of Egypt.]

Acknowledgments

The authors would like to thank the Fundación Ramón Areces, in the hallmark of the META2NOL project granted in the XIX national call of life and matter sciences projects, grant number CIVP19A5952. Also, the author, Ahmad Abo Markeb, appreciated and would like to thank the Ministry of Higher Education of Egypt for the Post-doc (6 months short-mission) grant.

Appendix A. Supplementary material

Supplementary data to this article can be found online at https://doi.org/10.1016/j.arabjc.2023.105022.

References

Abdi Hassan, A., Tanimu, A., Ganiyu, S.A., Yaagoob, I.Y., et al, 2022. Selective removal of Cd(II), As(III), Pb(II) and Cr(III) ions from water resources using novel 2-anthracene ammonium-based magnetic ionic liquids. Arab. J. Chemistry 15, (10). https://doi.org/10.1016/j.arabjc.2022.104136 104136.

Abo Markeb, A., Alonso, A., Sánchez, A., Font, X., 2017. Adsorption process of fluoride from drinking water with magnetic core-shell Ce-Ti@Fe_3O_4 and Ce-Ti oxide nanoparticles. Sci. Total Environ. 598, 949–958. https://doi.org/10.1016/j.scitotenv.2017.04.191.

Abo Markeb, A., Llimós-Turet, J., Ferrer, I., Blánquez, P., et al, 2019. The use of magnetic iron oxide based nanoparticles to improve microalgae harvesting in real wastewater. Water Res. 159, 490–500. https://doi.org/10.1016/j.watres.2019.05.023.

Afolabi, F.O., Musonge, P., Bakare, B.F., 2021. Application of the response surface methodology in the removal of Cu^{2+} and Pb^{2+} from aqueous solutions using orange peels. Sci. Afr. 13, e00931.

Bagbi, Y., Sarswat, A., Mohan, D., Pandey, A., et al, 2017. Lead and chromium adsorption from water using L-Cysteine functionalized magnetite (Fe_3O_4) nanoparticles. Sci. Rep. 7 (1), 7672. https://doi.org/10.1038/s41598-017-03380-x.

Bao, S., Li, K., Ning, P., Peng, J., et al, 2017. Highly effective removal of mercury and lead ions from wastewater by mercaptoamine-functionalised silica-coated magnetic nano-adsorbents: behaviours and mechanisms. Appl. Surf. Sci. 393, 457–466. https://doi.org/10.1016/j.apsusc.2016.09.098.

Burakov, A.E., Galunin, E.V., Burakova, I.V., Kucherova, A.E., et al, 2018. Adsorption of heavy metals on conventional and nanostructured materials for wastewater treatment purposes: a review. Ecotoxicol. Environ. Saf. 148, 702–712. https://doi.org/10.1016/j.ecoenv.2017.11.034.

Cai, Y., Yuan, F., Wang, X., Sun, Z., et al, 2017. Synthesis of core–shell structured Fe_3O_4@carboxymethyl cellulose magnetic composite for highly efficient removal of Eu(III). Cellulose 24 (1), 175–190. https://doi.org/10.1007/s10570-016-1094-8.

Chen, K., He, J., Li, Y., Cai, X., et al, 2017. Removal of cadmium and lead ions from water by sulfonated magnetic nanoparticle adsorbents. J. Colloid Interface Sci. 494, 307–316. https://doi.org/10.1016/j.jcis.2017.01.082.

Chu, Y., Zhang, X., Chen, W., Wu, F., et al, 2019. Plasma assisted-synthesis of magnetic TiO_2/SiO_2/Fe_3O_4-polyacrylic acid microsphere and its application for lead removal from water. Sci. Total Environ. 681, 124–132. https://doi.org/10.1016/j.scitotenv.2019.05.064.

Danalıoğlu, S.T., Kerkez Kuyumcu, Ö., Abdel Salam, M., Bayazit, Ş. S., 2018. Chitosan grafted SiO_2–Fe_3O_4 nanoparticles for removal of antibiotics from water. Environ. Sci. Pollut. Res. 25 (36), 36661–36670. https://doi.org/10.1007/s11356-018-3573-y.

Das, C., Singh, S., Bhakta, S., Mishra, P., et al, 2022. Bio-modified magnetic nanoparticles with Terminalia arjuna bark extract for the removal of methylene blue and lead (II) from simulated wastewater. Chemosphere 291,. https://doi.org/10.1016/j.chemosphere.2021.132673 132673.

Davodi, B., Jahangiri, M., Ghorbani, M., 2020. The lead removal from aqueous solution by magnetic Fe_3O_4@polydopamine nanocomposite using Box-Behnken design. Part. Sci. Technol. 38 (3), 325–336. https://doi.org/10.1080/02726351.2018.1539796.

Dermanaki Farahani, S., Zolgharnein, J., 2021. Multivariate optimization of high removal of lead(II) using an efficient synthesized Ni-based metal–organic framework adsorbent. Chin. J. Chem. Eng. 29, 146–153. https://doi.org/10.1016/j.cjche.2020.08.011.

Dong, Z., Yang, Y., Cai, X., Tang, X., et al, 2022. Site-selective synthesis of an amine-functionalized β-ketoenamine-linked covalent organic framework for improved detection and removal of Cu^{2+} ion from water. J. Solid State Chem. 316,. https://doi.org/10.1016/j.jssc.2022.123644 123644.

Eren, E., Afsin, B., Onal, Y., 2009. Removal of lead ions by acid activated and manganese oxide-coated bentonite. J. Hazard. Mater. 161 (2), 677–685. https://doi.org/10.1016/j.jhazmat.2008.04.020.

Fato, F.P., Li, D.-W., Zhao, L.-J., Qiu, K., et al, 2019. Simultaneous removal of multiple heavy metal ions from river water using ultrafine mesoporous magnetite nanoparticles. ACS Omega 4 (4), 7543–7549. https://doi.org/10.1021/acsomega.9b00731.

Goel, J., Kadirvelu, K., Rajagopal, C., Kumar Garg, V., 2005. Removal of lead(II) by adsorption using treated granular activated carbon: Batch and column studies. J. Hazard. Mater. 125 (1), 211–220. https://doi.org/10.1016/j.jhazmat.2005.05.032.

Gong, R., Ding, Y., Liu, H., Chen, Q., et al, 2005. Lead biosorption and desorption by intact and pretreated spirulina maxima biomass. Chemosphere 58 (1), 125–130. https://doi.org/10.1016/j.chemosphere.2004.08.055.

Gong, J., Wang, X., Shao, X., Yuan, S., et al, 2012. Adsorption of heavy metal ions by hierarchically structured magnetite-carbonaceous spheres. Talanta 101, 45–52. https://doi.org/10.1016/j.talanta.2012.08.035.

Hu, R., Wang, X., Dai, S., Shao, D., et al, 2015. Application of graphitic carbon nitride for the removal of Pb(II) and aniline from aqueous solutions. Chem. Eng. J. 260, 469–477. https://doi.org/10.1016/j.cej.2014.09.013.

Huang, Q., Zhang, Y., Zhou, W., Huang, X., et al, 2021. Amorphous molybdenum sulfide mediated EDTA with multiple active sites to boost heavy metal ions removal. Chin. Chem. Lett. 32 (9), 2797–2802. https://doi.org/10.1016/j.cclet.2020.12.020.

Huang, Y., Zheng, H., Hu, X., Wu, Y., et al, 2022. Enhanced selective adsorption of lead(II) from complex wastewater by DTPA functionalized chitosan-coated magnetic silica nanoparticles based on anion-synergism. J. Hazard. Mater. 422,. https://doi.org/10.1016/j.jhazmat.2021.126856 126856.

Ihsanullah, A., Abbas, A.M., Al-Amer, T.L., et al, 2016. Heavy metal removal from aqueous solution by advanced carbon nanotubes: critical review of adsorption applications. Sep. Purif. Technol. 157, 141–161. https://doi.org/10.1016/j.seppur.2015.11.039.

Jaihan, W., Mohdee, V., Sanongraj, S., Pancharoen, U., et al, 2022. Biosorption of lead (II) from aqueous solution using Cellulose-based Bio-adsorbents prepared from unripe papaya (Carica papaya) peel waste: removal Efficiency, Thermodynamics, kinetics and isotherm analysis. Arab. J. Chem. 15, (7). https://doi.org/10.1016/j.arabjc.2022.103883 103883.

Jin, X., Wang, G.-Q., Ma, D., Deng, S.-Q., et al, 2019. Cationic amorphous metal-organic cage-based materials for the removal of oxo-anions from water. ACS Appl. Nano Mater. 2 (9), 5824–5832. https://doi.org/10.1021/acsanm.9b01294.

Karatas, M., 2012. Removal of Pb(II) from water by natural zeolitic tuff: Kinetics and thermodynamics. J. Hazard. Mater. 199–200, 383–389. https://doi.org/10.1016/j.jhazmat.2011.11.035.

Karimi-Shamsabadi, M., Nezamzadeh-Ejhieh, A., 2016. Comparative study on the increased photoactivity of coupled and supported manganese-silver oxides onto a natural zeolite nano-particles. J. Mol. Catal. A: Chemical 418–419, 103–114. https://doi.org/10.1016/j.molcata.2016.03.034.

Karunanayake, A.G., Todd, O.A., Crowley, M., Ricchetti, L., et al, 2018. Lead and cadmium remediation using magnetized and nonmagnetized biochar from Douglas fir. Chem. Eng. J. 331, 480–491. https://doi.org/10.1016/j.cej.2017.08.124.

Kolluru, S.S., Agarwal, S., Sireesha, S., Sreedhar, I., et al, 2021. Heavy metal removal from wastewater using nanomaterials-process and engineering aspects. Process Saf. Environ. Prot. 150, 323–355. https://doi.org/10.1016/j.psep.2021.04.025.

Kurnaz Yetim, N., Kurşun Baysak, F., Koç, M.M., Nartop, D., 2020. Characterization of magnetic Fe_3O_4@SiO_2 nanoparticles with fluorescent properties for potential multipurpose imaging and theranostic applications. J. Mater. Sci.: Mater. Electron. 31 (20), 18278–18288. https://doi.org/10.1007/s10854-020-04375-7.

Lee, Y.-C., Yang, J.-W., 2012. Self-assembled flower-like TiO_2 on exfoliated graphite oxide for heavy metal removal. J. Indust. Eng. Chem. 18 (3), 1178–1185. https://doi.org/10.1016/j.jiec.2012.01.005.

Li, G., Ye, J., Fang, Q., Liu, F., 2019. Amide-based covalent organic frameworks materials for efficient and recyclable removal of heavy metal lead (II). Chem. Eng. J. 370, 822–830. https://doi.org/10.1016/j.cej.2019.03.260.

Liu, G., Liao, L., Dai, Z., Qi, Q., et al, 2020. Organic adsorbents modified with citric acid and Fe_3O_4 enhance the removal of Cd and Pb in contaminated solutions. Chem. Eng. J. 395,. https://doi.org/10.1016/j.cej.2020.125108 125108.

Liu, J., Zhou, J., Wu, Z., Tian, X., et al, 2022. Concurrent elimination and stepwise recovery of Pb(II) and bisphenol A from water using β–cyclodextrin modified magnetic cellulose: adsorption performance and mechanism investigation. J. Hazard. Mater. 432,. https://doi.org/10.1016/j.jhazmat.2022.128758 128758.

Mahmoud, M.E., Abdel-Fattah, T.M., Osman, M.M., Ahmed, S.B., 2012. Chemically and biologically modified activated carbon sorbents for the removal of lead ions from aqueous media. J. Environ. Sci. Health, Part A 47 (1), 130–141. https://doi.org/10.1080/10934529.2012.630292.

Mahmoud, M.E., Abdelwahab, M.S., Abdou, A.E.H., 2016. Enhanced removal of lead and cadmium from water by Fe_3O_4-cross linked-O-phenylenediamine nano-composite. Sep. Sci. Technol. 51 (2), 237–247. https://doi.org/10.1080/01496395.2015.1093505.

Mahmoud, M.E., Ibrahim, G.A.A., Abdelwahab, M.S., 2021. Manganese dioxide nanoparticles decorated with chitosan for effective removal of lead and lanthanum ions from water by microwave sorption technique. Mater. Sci. Eng. B 267,. https://doi.org/10.1016/j.mseb.2021.115091 115091.

Maliyekkal, S.M., Lisha, K.P., Pradeep, T., 2010. A novel cellulose–manganese oxide hybrid material by in situ soft chemical synthesis and its application for the removal of Pb(II) from water. J. Hazard. Mater. 181 (1), 986–995. https://doi.org/10.1016/j.jhazmat.2010.05.112.

Mehdinia, A., Niroumand, R., Jabbari, A., 2020. Removal of lead and copper ions from environmental water samples by nanorattle magnetic polypyrrole. Int. J. Environ. Sci. Technol. 17 (5), 2721–2730. https://doi.org/10.1007/s13762-019-02565-3.

Morsy, M., Mostafa, K., Amyn, H., El-Ebissy, A.-A.-H., et al, 2019. Synthesis and Characterization of Freeze Dryer Chitosan Nano particles as Multi functional Eco-Friendly Finish for Fabricating Easy Care and Antibacterial Cotton Textiles. Egypt. J. Chem. 62 (7), 1277–1293. https://doi.org/10.21608/EJCHEM.2019.6995.1583.

Ozdes, D., Gundogdu, A., Kemer, B., Duran, C., et al, 2009. Removal of Pb(II) ions from aqueous solution by a waste mud from copper mine industry: Equilibrium, kinetic and thermodynamic study. J. Hazard. Mater. 166 (2), 1480–1487. https://doi.org/10.1016/j.jhazmat.2008.12.073.

Park, J.O., Rhee, K.Y., Park, S.J., 2010. Silane treatment of Fe_3O_4 and its effect on the magnetic and wear properties of Fe_3O_4/epoxy nanocomposites. Appl. Surf. Sci. 256 (23), 6945–6950. https://doi.org/10.1016/j.apsusc.2010.04.110.

Patel, H., 2021. Review on solvent desorption study from exhausted adsorbent. J. Saudi Chem. Soc. 25, (8). https://doi.org/10.1016/j.jscs.2021.101302 101302.

Perez, T., Pasquini, D., de Faria Lima, A., Rosa, E.V., et al, 2019. Efficient removal of lead ions from water by magnetic nanosorbents based on manganese ferrite nanoparticles capped with thin layers of modified biopolymers. J. Environ. Chem. Eng. 7, (1). https://doi.org/10.1016/j.jece.2019.102892 102892.

Rajput, S., Pittman, C.U., Mohan, D., 2016. Magnetic magnetite (Fe_3O_4) nanoparticle synthesis and applications for lead (Pb^{2+}) and chromium (Cr^{6+}) removal from water. J. Colloid Interface Sci. 468, 334–346. https://doi.org/10.1016/j.jcis.2015.12.008.

Recillas, S., García, A., González, E., Casals, E., et al, 2011. Use of CeO_2, TiO_2 and Fe_3O_4 nanoparticles for the removal of lead from water: Toxicity of nanoparticles and derived compounds. Desalination 277 (1), 213–220. https://doi.org/10.1016/j.desal.2011.04.036.

Renu, M.A., Singh, K., 2016. Heavy metal removal from wastewater using various adsorbents: a review. J. Water Reuse Desalin. 7 (4), 387–419. https://doi.org/10.2166/wrd.2016.104.

Rodríguez, A.R.C., McCarthy, J.E., Alonso, A., Moral-Vico, J., et al, 2018. Cerium oxide nanoparticles anchored onto graphene oxide for the removal of heavy metal ions dissolved in water. Desalination Water Treat. 124, 134–145. https://doi.org/10.5004/dwt.2018.22735.

Sadegh, H., Ali, G.A.M., Gupta, V.K., Makhlouf, A.S.H., et al, 2017. The role of nanomaterials as effective adsorbents and their applications in wastewater treatment. J. Nanostructure Chem. 7 (1), 1–14. https://doi.org/10.1007/s40097-017-0219-4.

Shi, W.-Y., Shao, H.-B., Li, H., Shao, M.-A., et al, 2009. Progress in the remediation of hazardous heavy metal-polluted soils by natural zeolite. J. Hazard. Mater. 170 (1), 1–6. https://doi.org/10.1016/j.jhazmat.2009.04.097.

Shi, Q., Terracciano, A., Zhao, Y., Wei, C., et al, 2019. Evaluation of metal oxides and activated carbon for lead removal: kinetics, isotherms, column tests, and the role of co-existing ions. Sci. Total Environ. 648, 176–183. https://doi.org/10.1016/j.scitotenv.2018.08.013.

Shoukry, A., Hosny, W., 2012. Coordination properties of N, O-carboxymethyl chitosan (NOCC). Synthesis and equilibrium studies of some metal ion complexes. Ternary complexes involving Cu (II) with (NOCC) and some biorelevant ligand. Cent. Eur. J. Chem. 10 (1), 59–70. https://doi.org/10.2478/s11532-011-0116-5.

Singh, R., Bhateria, R., 2020. Experimental and modeling process optimization of lead adsorption on magnetite nanoparticles via isothermal, kinetics, and thermodynamic studies. ACS Omega 5 (19), 10826–10837. https://doi.org/10.1021/acsomega.0c00450.

Wang, L., Li, J., Jiang, Q., Zhao, L., 2012. Water-soluble Fe_3O_4 nanoparticles with high solubility for removal of heavy-metal ions from waste water. Dalton Trans. 41 (15), 4544–4551. https://doi.org/10.1039/C2DT11827K.

Xiong, C., Wang, S., Hu, P., Huang, L., et al, 2020. Efficient Selective Removal of Pb(II) by Using 6-Aminothiouracil-Modified Zr-Based Organic Frameworks: From Experiments to Mechanisms. ACS Appl. Mater. Interfaces 12 (6), 7162–7178. https://doi.org/10.1021/acsami.9b19516.

Xu, J., Ju, C., Sheng, J., Wang, F., et al, 2013. Synthesis and characterization of magnetic nanoparticles and its application in lipase immobilization. Bull. Korean Chem. Soc. 34 (8), 2408–2412. https://doi.org/10.5012/bkcs.2013.34.8.2408.

Yang, L., Wen, T., Wang, L., Miki, T., et al, 2019. The stability of the compounds formed in the process of removal Pb(II), Cu(II) and Cd (II) by steelmaking slag in an acidic aqueous solution. J. Environ. Manage. 231, 41–48. https://doi.org/10.1016/j.jenvman.2018.10.028.

Yasmeen, K., Nawaz, S., Iqbal, A., Siddiqui, A., et al, 2022. Removal of Pb(II) from water samples using surface modified core/shell CdZnS/ZnS QDs as adsorbents: Characterization, adsorption, kinetic and thermodynamic studies. Arab. J. Chem. 15, (11). https://doi.org/10.1016/j.arabjc.2022.104224 104224.

Zhang, B.-L., Qiu, W., Wang, P.-P., Liu, Y.-L., et al, 2020. Mechanism study about the adsorption of Pb(II) and Cd(II) with iron-trimesic metal-organic frameworks. Chem. Eng. J. 385,. https://doi.org/10.1016/j.cej.2019.123507 123507.